A Comparative Study of Pomegranate Sb@C Yolk-Shell Microspheres as Li and Na-Ion Battery Anodes

Journal:	*Nanoscale*
Manuscript ID	NR-ART-10-2018-008461.R1
Article Type:	Paper
Date Submitted by the Author:	15-Nov-2018
Complete List of Authors:	Song, Junhua; Washington State University, School of Mechanical and Materials Engineering Xiao, Dongdong; Pacific Northwest National Laboratory Jia, Haiping; Pacific Northwest National Laboratory Zhu, Guomin; Pacific Northwest National Laboratory Engelhard, Mark; Pacific Northwest National laboratory, Environmental Molecular Sciences Laboratory Xiao, Biwei; Pacific Northwest National Laboratory Feng, Shuo; Washington State University, Mechanical and Materials Engineering Li, Dongsheng; Pacific Northwest National Laboratory Reed, David; Pacific Northwest National Laboratory Sprenkle, Vincent; Pacific Northwest National Laboratory, Lin, Yuehe; Washington State University, School of Mechanical and Materials Engineering Li, Xiaolin; Pacific Northwest National Laboratory,

SCHOLARONE™
Manuscripts

A Comparative Study of Pomegranate Sb@C Yolk-Shell Microspheres as Li and Na-Ion Battery Anodes

Junhua Song[1,2], Dongdong Xiao[1], Haiping Jia[1], Guomin Zhu[1], Mark Engelhard[1], Biwei Xiao[1], Shuo Feng[2], Dongsheng Li[1], David Reed[1], Vincent L. Sprenkle[1], Yuehe Lin[2] and Xiaolin Li[1*]*

1. Pacific Northwest National Laboratory, 902 Battelle Boulevard Richland, WA, 99354, USA

2. School of Mechanical and Materials Engineering, Washington State University, Pullman, WA 99164, USA

ABSTRACT

Alloy-based anodes of nanostructure have the privilege of alleviating the challenges of the large volume expansion and improving the cycling stability and rate performance for high energy lithium- and sodium-ion batteries (LIBs and SIBs). Yet, it faces the dilemma of worsening the parasitic reactions at the electrode-electrolyte interface and low pack density for practical electrode fabrication. Here, pomegranate Sb@C yolk-shell microspheres were developed as a high-performance anode for LIBs and SIBs with controlled interfacial properties and enhanced packing density. Although the same yolk-shell nanostructure (primary particle size, porosity) and three-dimensional architecture alleviated the volume change induced stress and swelling in both batteries, the SIB shows 99% capacity retention over 200 cycles, much better than the 78% capacity retention of LIBs. The comparative electrochemical study and X-ray photoelectron

spectroscopy characterization revealed that the different SEI, besides the distinct phase transition mechanism, played a critical role in the divergent cycling performance.

1. INTRODUCTION

Li- and Na-ion batteries (LIBs and SIBs) are the twin analogies explored in the 80s for high energy electrochemical storage devices.[1, 2] LIBs continue its success today by supporting a variety of electrified portable devices and transportation applications.[3] Meanwhile, the rapidly expanding integration of renewable energy has stirred up the quest for more economically viable energy storage systems than LIBs. Although falling short of the high energy density, SIBs, accredited to their natural abundance of the precursor, uniform geological distribution and low cost, still are being regarded as one of the leading rechargeable energy storage technologies for grid-scale storage systems.[4-6] To better serve the purposes in their own respective applications, LIBs and SIBs need to acquire higher energy density and better cyclability than the corresponding state-of-the-art devices, respectively. Using high capacity alloy-typed anodes is one of the promising ways to boost the energy density of LIBs and SIBs. Upon full lithiation or sodiation, alloys and their intermetallic compounds, such as, FeS_2, SnO_2, Sn, SnS, Sn_4P_3, Si, Ge, Sb and NiSb can deliver 2-10 times higher specific capacity than natural graphite or hard carbon anodes.[7-16] Integrated with proper cell design/engineering, the energy density of the full cells with alloy anodes can be greatly improved.

Antimony (Sb) stands out with high specific capacity and reasonable alloying/dealloying potential as anodes for both Li and Na-ion batteries.[17] Interestingly, the cycling stability of Sb anode is different in LIBs and SIBs, despite the many similarities shared between these two neighboring

alkali ions.[18] Early research on the cyclability of Sb has pointed to the different phase transition pathways between the Na and Li systems, leading to dissimilar rate of structural breakdown upon volume change.[18] Yet, the bulk Sb without any nanostructure induces large stress variation to the electrode integrity and unstable solid-electrolyte-interphase (SEI) layer, susceptible to the large volume change and severe interphasial reactions with electrolyte during cycling. Yolk-shell structured materials can effectively alleviate the volume change of alloy-type anode materials and provide electrode mechanical and electrical integrity.[19, 20] Recently, we developed a Sb@C yolk-shell structure, which demonstrated good cycling stability and rate performance for Na-ion intercalation.[21] Here, we further advance the technology to prepare pomegranate Sb@C yolk-shell microspheres (Sb@C MSs), which not only is a high density anode material for LIBs and SIBs, but also can act as a model material to systematically examine the stability difference for alloying/dealloying with Li and Na. The Sb@C MSs have appropriately controlled porosity to accommodate the volume change and maintain a high packing density of ~1.1 g cm^{-3}, which is ~40% of the value of Sb particles of ~70 micrometers (~2.63 mg cm^{-3}) and 30% larger than the Sb@C yolk-shell structures. The anode exhibits good electrochemical performance in terms of specific capacity and rate capability for both Li-ion and Na-ion cells. The specific capacities for Li- and Na-ion batteries at low current density of 50 mA g^{-1} are close to theoretical values of 935 mAh g^{-1} and 637 mAh g^{-1}. It can still deliver 633 mAh g^{-1} and 441 mAh g^{-1}, respectively, at the current density of 5 A g^{-1}. The SIBs show incredibly good cycling stability with 99% capacity retention over 200 cycles at the current density of 200 mA g^{-1}, while the LIBs demonstrated ~78% capacity retention at similar condition. The different electrochemical behaviors in Li and Na cells

are systematically investigated to reveal their alloying mechanism, cell impedance evolution, SEI composition and thickness during cycling.

2. EXPERIMENTAL SECTION

2.1 Synthesis of pomegranate Sb@C yolk-shell microspheres (Sb@C MS)

In a typical synthesis, ~400 mg of Sb_2O_3 nanoparticles (Sigma-Aldrich) was dispersed into 200 ml of Tris-buffer solution (10 mM, pH=8.5, Biotech) and sonicated for 30 minutes. Then dopamine (Sigma-Aldrich) of 400 mg was added into the above solution and mechanically stirred overnight to obtain polydopamine (PDA) coated Sb_2O_3 nanoparticle (Sb_2O_3@PDA). The resultant Sb_2O_3@PDA core-shell structure was then dispersed in 200 ml polyvinylpyrrolidone (PVP, average molecular weight 40,000, Sigma-Aldrich) solution (10 mg/ml) and stirred for 6 hr. Excess PVP was removed by washing the Sb_2O_3@PDA with distilled water twice. To coat the Sb_2O_3@PDA with SiO_2, the PVP functionalized Sb_2O_3@PDA was dispersed into a 400 ml ethanol/water solution (4:1 by volume) with the addition of 4 ml NH_4OH (28-30%, Sigma-Aldrich) and 1.2 ml tetraethyl orthosilicate (TEOS, 98%, Sigma-Aldrich) in sequence. The resultant Sb_2O_3@PDA@SiO_2 was washed for several times and re-dispersed to form a 40 mg/ml aqueous solution.

The emulsion was prepared by adding 1 g of Hypermer emulsifier (Hypermer™ 2524, Croda USA) into ~400 ml of 1-octadecene (ODE) and stirring for 20 minutes to form a homogeneous solution. The Sb_2O_3@PDA@SiO_2 precursor solution (~2 ml) was then mixed with 8 ml ODE solution and emulsified using a homogenizer for 1 minute. The micron sized Sb_2O_3@PDA@SiO_2 was obtained after water evaporation at 95 °C for 6 hr followed by several washing cycles with petroleum ether. To stabilize the structure, the micron sized Sb_2O_3@PDA@SiO_2 was further coated with another

layer of PDA Finally, the Sb@C MSs yolk-shell was obtained by thermal treatment the sample at 480 $^{\circ}$C in Ar/H$_2$ (5%) for 1 hr and subsequent HF etching to remove the SiO$_2$ layer and Sb$_2$O$_3$ residual.

2.2 Characterization

Crystal structure characterization of the cycled electrode was carried out on a Rigaku MiniFlex 600 X-ray diffraction (XRD) instrument operated at 40 kV accelerating voltage and a current of 15 mA. The morphological and elemental analysis of the sample were conducted on a field emission scanning electron microscope (SEM) with an energy dispersive spectroscopy (EDS) and an electron transmission microscope (Technai G2 F20, FEI Company) equipped with a scanning transmission electron microscopy (STEM) unit. The X-ray photoelectron spectroscopy (XPS) was taken on the cycled electrode at desodiated state using a Physical Electronics Quantera Scanning X-ray Microprobe. A focused monochromatic Al Kα X-ray (1486.7 eV) source was equipped for excitation. The packing density analysis was done by adding equally weighted Sb@C yolk-shell structure, Sb@C MSs and bulk Sb (200 mesh, Alfa-Aesar) powders into glass tubes and shaken for 30 minutes using an electrical vibrator. The volumetric density was calculated based on the mass and volume of the powders.

2.3 Electrochemical testing

The electrode of pomegranate Sb@C MS yolk-shell material was prepared by slurry casting the mixture of active material, Super-P and sodium carboxymethyl cellulose (CMC) with a mass ratio of 60:20:20. The slurry then was casted on copper foil and dried under vacuum at 70 °C for 12 hr.

The half-cell (2032 coin cell from MTI Corp) was assembled in an argon-filled glove box with Celgard 3501 as separator and sodium foil as the counter electrode. The electrolyte was 1 M $NaClO_4$ in ethylene carbonate (EC)/dimethyl carbonate (DMC) (1:2 by weight) with 10 wt.% fluoroethylene carbonate (FEC) and the amount was kept at 100 μL unless otherwise mentioned. The average active material loading was ~1 to 2 mg•cm^{-2}. The electrodes were tested on an Arbin BT-2000 battery tester at the charge-discharge potential range of 0.02-2.0 V vs. Na^+/Na and vs. Li^+/Li for SIBs and LIBs, respectively. The capacity was calculated based on the weight of the Sb@C MS composite. The cell internal resistance was measured using galvanostatic intermittent titration technique (GITT) by applying a pulse current with 10 minutes duration, followed by 30 minutes pause time. The electrochemical impedance spectra (EIS) were measured on impedance analyzer (Solatron Analytical).

**3. RESULTS AND DISCUSSION**
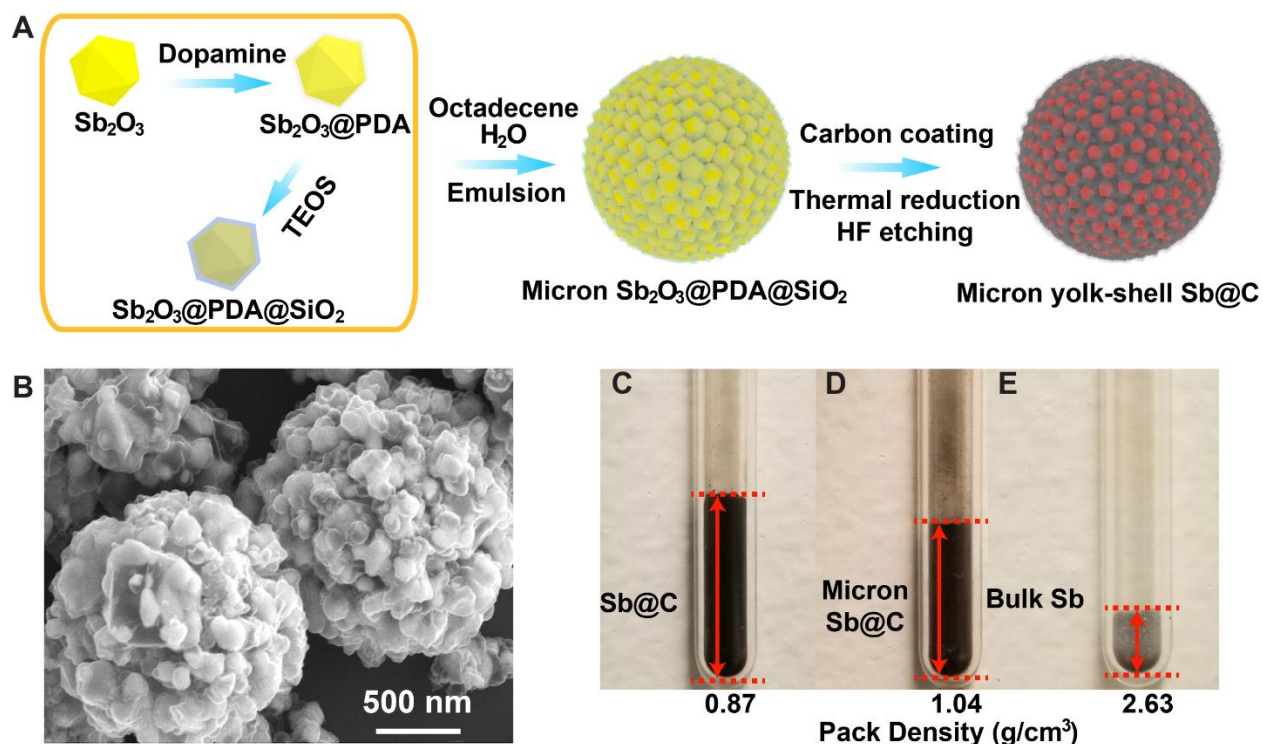
Figure 1. Pomegranate Sb@C yolk-shell microspheres (Sb@C MSs). (A) Schematic illustration of the synthesis of Sb@C MSs. (B) SEM image of typical Sb@C MSs. Pack density comparison of (C) nano-Sb@C yolk-shell structure, (D) Sb@C MSs and (E) bulk Sb of ~70 micrometers.

The Sb@C MSs are synthesized through a micro-emulsion method assisted controlled reduction and etching of $Sb_2O_3@C@SiO_2$ core-shell structure. As depicted in the schematic illustration in Figure 1A, the $Sb_2O_3@PDA@SiO_2$ core-shell structure was prepared as primary particles by coating commercial Sb_2O_3 nanoparticles with layers of polydopamine and silica in sequence. Then they were assembled into microspheres, partially reduced and etched with HF forming microspheres of Sb@C yolk-shell structure. The transmission electron microscopy (TEM) and scanning transmission electron microscopy (STEM) images in Figures S1 were taken on a typical $Sb_2O_3@PDA@SiO_2$ particle. The Sb, C, N, and Si elemental mapping (Figure S1) clearly revealed the uniform coating layers of polydopamine and SiO_2 on the Sb_2O_3 particles. The Sb@C yolk shell

microspheres were obtained by drying the emulsified micro-droplet of $Sb_2O_3@PDA@SiO_2$ in a water-in-oil system, carbonization of the polymer, thermal reduction of the Sb_2O_3 into Sb and subsequent etching of SiO_2 and Sb_2O_3. By controlling the SiO_2 layer thickness and reduction temperature, the resultant Sb@C MS consists of myriads of yolk-shell particles that allow the nano Sb to expand within the electrically conductive carbon shell. The obtained Sb@C MSs possess a similar crystallographic structure and Sb content as our previous report (Figure S2).[21] Figure 1B shows the representative scanning electron microscopy (SEM) image of the Sb@C MSs, in which nano Sb@C yolk shell particles were self-assembled and interlocked together in the H_2O/octadecene microemulsion system. The average secondary particle sizes of Sb@C MSs are ~2 to 10 μm, a good range for battery materials processing (Figure 1B and Figures S3). [22, 23] The Sb particle size is ~100-200 nm and the gap is ~50-200 nm from the Sb@C yolk shell particles at the surface of the microspheres (Figure 1B) and TEM images of a broken microsphere (Figure S3). The Sb@C MSs are expected to not only have the advantage of controlled porosity in accommodating the volume change of Sb, similar to nano Sb@C yolk-shell particles, but also improved tap density, minimized surface area and mitigated parasitic reactions of electrolyte decomposition. Side-by-side comparison of the packing density of the Sb@C microspheres, nano Sb@C yolk-shell particles, and bulk Sb (74μm) was scrutinized in Figures 1C-1E. Naturally, bulk Sb showed the highest pack density of 2.63 g cm^{-3}. The Sb@C MSs demonstrated a packing density of ~ 1.08 g cm^{-3}, ~41% of bulk Sb and ~30% more than the nano Sb@C yolk-shell particle's density (0.87 g cm^{-3}). It has to be noted that for alloy anodes of large swell, the electrode density at the 100% state of lithiation/sodiation is more meaningful in practice than the density after electrode manufacturing. The theoretical volume expansion of fully lithiated/sodiated Sb is around 135%

(Li) and 293% (Na), which will decrease the pack density of bulk Li_3Sb/Na_3Sb to ~1.94/0.9 g cm^{-3}, respectively.[24] This is close to the density of Sb@C yolk shell microspheres.[21] The density measurement corroborates the pore volume control in our Sb@C yolk-shell MSs is very close to the optimized value in accommodating the volume expansion of Sb during sodiation or lithiation. TEM and the energy dispersive X-ray (EDX) elemental mapping of a broken part of a Sb@C microsphere in Figure S3D-H further confirm the uniform coating of the conductive carbon layer and the empty inner space deliberately left after removing the SiO_2 layer.
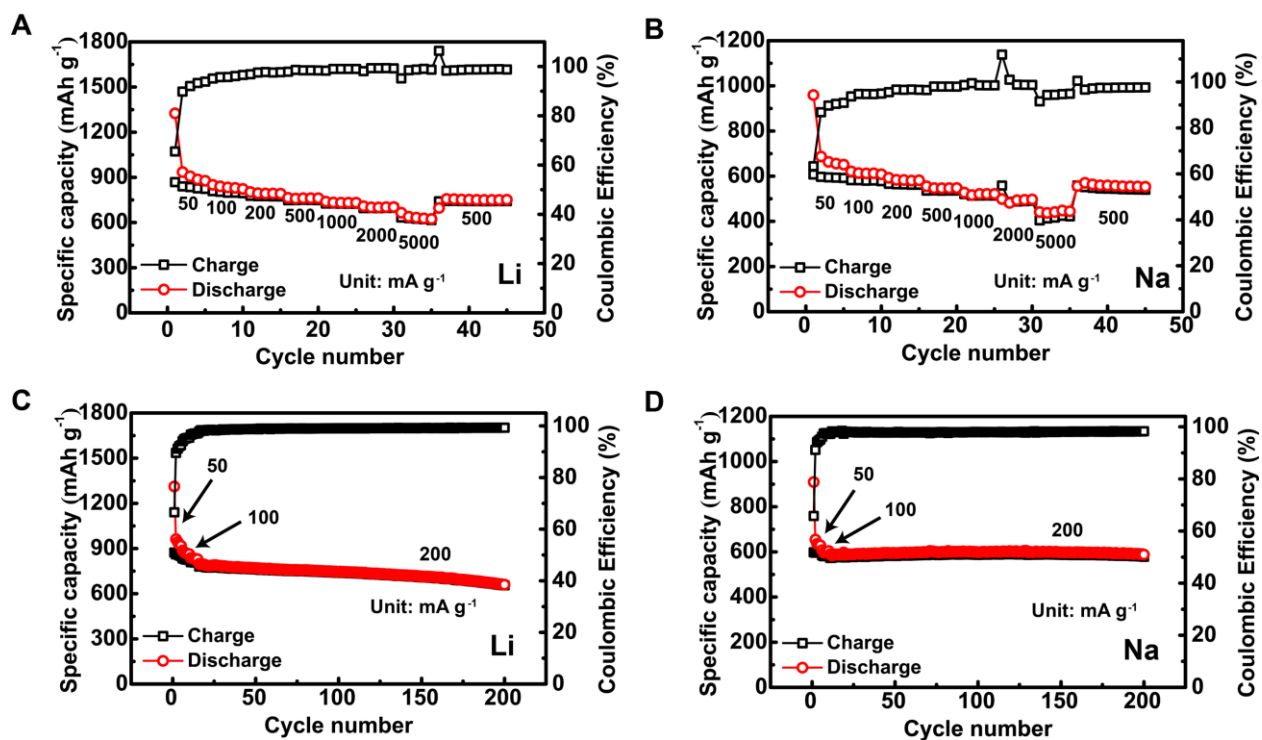
Figure 2. Typical electrochemical performance of the Sb@C MSs in Li- and Na-ion batteries. (A) Li-ion storage capacity at different current densities. (B) Na-ion storage capacity at different current densities. (C) Long term cycling of the Sb@C MS anodes against Li. (D) Long term cycling of the Sb@C MS anodes against Na.

The Sb@C MSs showed good electrochemical performance in both Li- and Na-ion batteries. Figure 2A shows the specific capacities of the Sb@C MS anodes in LIBs at various

charge/discharge current densities. The specific discharge capacities are ~935 mAh g^{-1} (2nd cycle),

762 mAh g^{-1}, and 633 mAh g^{-1} at the current densities of 50 mA g^{-1}, 500 mA g^{-1}, and 5 A g^{-1},

respectively. At the same current densities in SIBs, it delivers specific discharge capacities of 637

mAh g^{-1}, 521 mAh g^{-1}, and 441 mAh g^{-1} (Figure 2B). Furthermore, the Sb@C MS anodes show

good cycling stability. In LIBs, it retained ~78% of its initial capacity after 200 cycles at 200 mA g^{-1}

(Figure 2C). The cycling stability is even better for SIBs. In Figure 2D, the anode showed

amazingly stable cycling with 99% capacity retention over 200 cycles at similar current density

200 mA g^{-1}.

The cycling stability difference of Sb in SIBs and LIBs has been observed previously for bulk

particles. Bulk Sb showed better cycling stability upon sodiation than lithiation, in spite of the

larger volume expansion of Sb at full sodiation (293%) than at full lithiation (135%).[24] The

distinctive alloying mechanism of Na-Sb with the presence of amorphous intermediate phase

compared to Li-Sb system was ascribed to be the reason.[18, 21] However, it is missing the detail

understanding of how the different phase transition and amorphous alloy phase affect the

electrochemical performance.

Many factors affect the cycling performance of Sb: 1) Sb expands ~293% at full sodiation while it

only expands ~135% at full lithiation. The stress from the different volume change will affect the

mechanical, electrical integrity and hence cycling stability. 2) The specific capacity of Sb in SIBs

and LIBs is different. The potentially disparate kinetics of the alloying process of Li and Na may

lead to different depth of Sb material utilization at the same current density and hence

potentially unlike capacity retention at the same cycling life. 3) The different SEIs in SIBs and

LIBs, particularly entangled with different volume change, degree of electrolyte decomposition

and SEI properties. 4) Dissimilar reversible electrochemistry can be introduced through kinetic controlled method such as the use of nanostructure/amorphous materials to lower the energy/spatial barrier.

The presence of the amorphous intermediate phase in Na-Sb system may provide similar function of using nanostructured material by introducing more reversible electrochemistry because of the fast kinetics and low energy/spatial barrier. However, it does not rule out other factors. Our Sb@C MSs is a good platform for systematic investigation of the mechanism of cycling stability difference of Sb in SIBs and LIBs: 1) With the appropriate void space in accommodating the Sb volume change, the electrodes can maintain relatively good mechanical/electrical integrity during cycling. 2) The yolk-shell structure with micron size particles of reduced surface area has controlled parasitic reactions of electrolyte decomposition. 3) Electrochemical measurement showed the Sb@C MSs had similar and very good alloying kinetic with Li and Na. The LIBs and SIBs specific capacity at the current density of 5 A g^{-1} retained ~68% and 69% of their capacities at 50 mA g^{-1}, respectively. 4) The long-term cycling stability for LIB and SIB was compared at the same current density of 200 mA g^{-1}.

X-ray photoelectron spectroscopy (XPS) characterization and a comparative study of the electrochemical kinetics revealed that the different SEIs of Sb in LIBs and SIBs were crucial to their long-term cycling performance/failure mechanism besides the contrasting alloying mechanism.

Before investigating the SEI difference, galvanostatic intermittent titration technique (GITT) was carried out to study the thermodynamics and kinetics of these two battery systems to understand how the different phase change and amorphous alloy phase affect the electrochemical

performance (Figure 3). According to the results, Li-ion storage showed lower resistance than the alloying/de-alloying of Na ions even though Na-Sb system has the amorphous intermediate phase in the alloying process. For the Li and Na cells shown in Figure 3A and B, the over potential before and after current pulse gradually increases during the charge step, and fluctuates during the discharge step, which reflects the changing energy barriers at different alloying/dealloying stages. To gain a closer look at the reaction kinetics at different lithiation/sodiation degree, the cell internal resistances are derived by dividing the over potential by the pulse current. Although the resistance of both systems is low, the Na-cell's resistance is ~1.5 times higher than that of Li-cell's on average (Figure 3C). The development of internal resistance is closely related to the sodium/lithium diffusion through the SEI layer and alloy with Sb. The GITT results indicate that Na^+ ion migration inside Sb faces larger energy barrier associated with relatively high internal resistance and sharp increase of energy barrier (resistance bump) approaching the full sodiation state. The amorphous intermediate phase in SIBs did not help much on the reaction kinetics or the electrochemical reversibility.
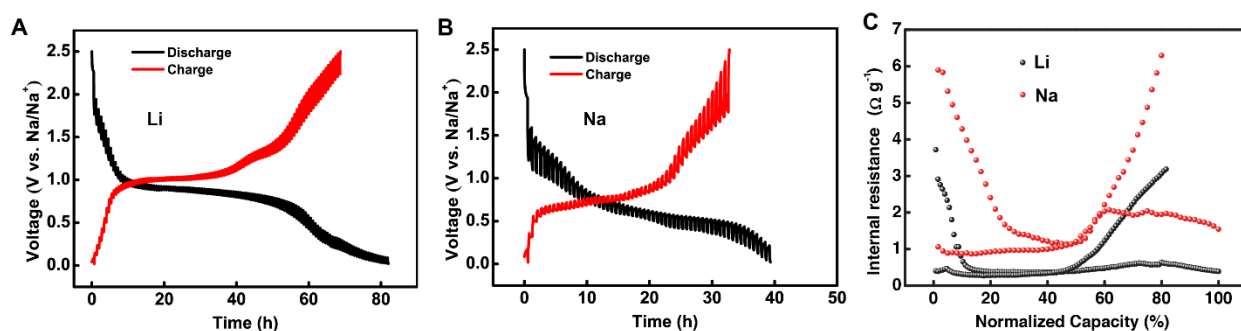

Figure 3. Galvanostatic intermittent titration technique (GITT) study of the alloying/de-alloying process of Sb in Li and Na ion batteries. (A) Typical GITT plot of a Li cell. (B) Typical GITT plot of a Na cell. (C) Comparison of reaction resistances of the Li (black dots) and Na (red dots) cell in (A) and (B).

Average Coulombic efficiency (CE) of the SIBs and LIBs provides indication of the reversibility of

the Li/Na ion storage process. At the same current density of 200 mA•g^{-1}, the average Coulombic

efficiency (CE) for the Sb@C MS-Na cell is ~97.73 %, lower than the value of a typical Sb@C MS-

Li cell, ~ 98.54 %. In fact, higher CE of Li cells holds true at different current densities in the rate

test. This indicates more parasitic reactions and SEI formation in the SIBs, while more reversible

electrochemical processes in LIBs. Parasitic reactions at the metal counter electrode also have

effect to the CE and it will be discussed in the electrochemical impedance spectroscopy (EIS)

study (vide infra).

More SEI on the Sb@C MS electrode surface in SIBs than in LIBs was corroborated by the XPS

characterization. Figure 4 showed the C, Cl and N XPS spectra of the electrodes after cycled for

200 times in LIBs and SIBs. The C 1s spectra (Figure 4A) reveal that electrodes from both systems

have very similar surface chemical composition consisting of sp^2 carbon, alkoxy and alkyl carbon,

fluorine contained groups and inorganic sodium salts.[25] The electrode cycled in the SIB has larger

ratio of SEI carbon: the sp^2 carbon than that in the LIB. The Cl signal is from the salt

decomposition. The Cl 2p spectrum from SIB presents a noticeable difference to its Li

counterpart, with stronger peak intensity in both ~200 eV (Cl$^-$) and 210 eV (ClO$_4^-$) regions (Figure

4B).[26] This indicates that the decomposition of Na salt is more dramatic than Li salt on the

electrode surface forming SEI. The accelerated salt decomposition might be the trigger point of

the swiftly thickening of SEI in the Na cell, which is evidenced by the N 1S spectra (Figure 4C).

Figure 4C showed that the nitrogen signal (~ 399.6 eV) from the carbonized polydopamine is

completely absent in the electrode from SIBs while it is sharp and clear in the electrode from

LIBs. Considering the XPS only reflected the surface information, the absence of nitrogen signal

can be ascribed to the thick SEI that covered up the carbon surface of Sb@C MSs cycled in SIBs.

In agreement with the XPS analysis, the SEM of cycled Na electrode (Figure S4A and B) shows less

recognizable Sb@C MSs than the cycled Li electrode (Figure S4C and D), as they are buried into a

thick SEI layer.
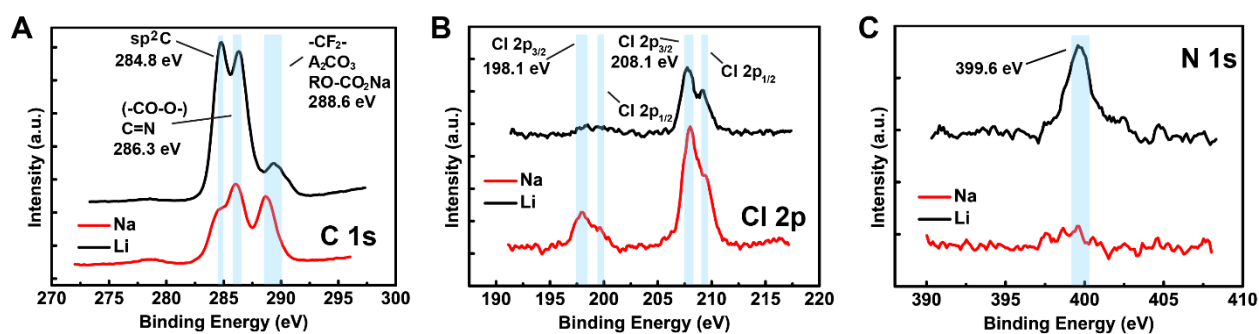
Figure 4. XPS spectra of Sb@C MS electrodes after 50 cycles in LIBs and SIBs. (A) C 1s spectra. (B)

Cl 2p spectra. (C) N 1s spectra.

The growth of SEI usually leads to the rising of cell impedance and subsequent cell failure or

capacity fade. Hence, the electrochemical impedance spectroscopy (EIS) was used to study the

SEI layer impedance evolution in the LIBs and SIBs. Figure 5 shows the representative Nyquist

plot of Li and Na cells at charged states before and after cycling. As we can see in Figures 5A and

5B, the SIB has larger impedance than the LIB before cycling.[27] Although the impedance decrease

after the 1st cycle, the SIB impedance is still larger than the LIB impedance (Figure 5C and 5D).

Detail comparison of the impedance evolution with cycling in both systems showed gradual

resistance increment in the charge-transfer (R_{ct}) region due to the development of SEI layer. The

impedance of the SIB increased for ~400% after 50 cycles while the impedance of LIBs increased

slightly by ~12% (Table S1).

The SEI impedance increment in the half cell against Li or Na metals, includes not only the structural degradation and SEI thickening on the Sb@C MSs' surface but also the metal surface. To avoid the effect from the counter metal anodes, the anodes after cycling in SIBs and LIBs for 150 cycles were disassembled and then re-assembled with fresh Li/Na metal anode. Figures 5E and 5F show that the impedance of both the SIB and LIB decreased. The R_{ct} impedance of the LIB only decreased slightly by 4 Ω, while the R_{ct} of SIB drops 188 Ω after switching to a fresh Na metal (Table S1). Even so, the SIB impedance is still much larger than the impedance of LIBs indicating more SEI on the Sb@C MSs' surface in SIBs. The large increase of the Na-Sb cell impedance did not lead to capacity fade, indicating SIBs are more tolerant to negative effect of the SEI growth.
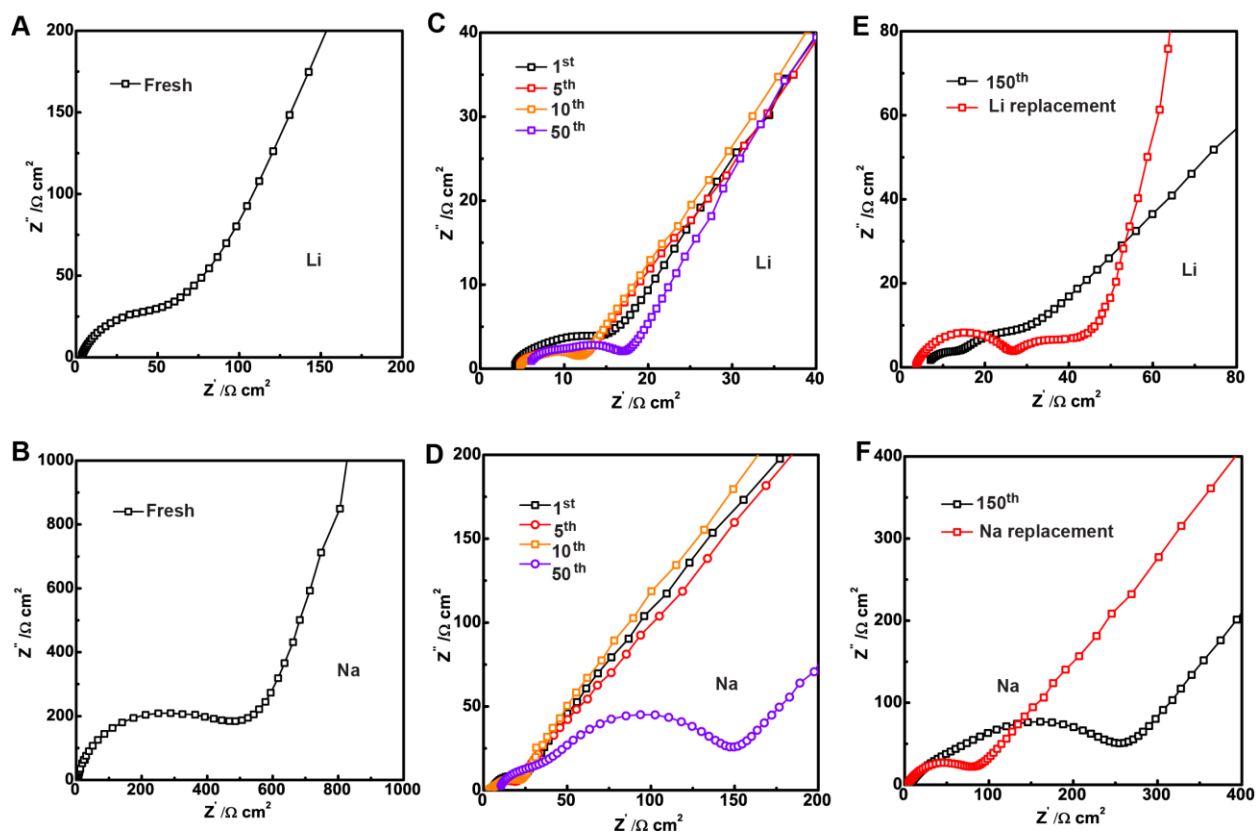
Figure 5. Impedance evolution of Sb@C MSs in LIBs and SIBs. (A) EIS of the LIB before cycling. (B) EIS of the SIB before cycling. (C) EIS comparison of the LIB after 1st, 5th, 10th and 50th cycles. (D)

EIS comparison of the SIB after 1st, 5th, 10th and 50th cycles. (E) EIS of the LIB after 150 cycles before and after switching to fresh Li metal. (F) EIS of the SIB after 150 cycles before and after switching to fresh Na metal.

On the basis of the above results from the battery testing, GITT, EIS and XPS, we can see that 1) although the intermediate phase of Na-Sb alloy is amorphous, the Na-Sb alloying process is more difficult than Li-Sb according to the larger resistance from GITT measurement and larger EIS impedance. The different alloying mechanism and the presence of amorphous interphase may help the cycling stability by releasing the stress, but does not help with the electrochemical reversibility. Since SIBs have more parasitic reactions than LIBs according to the CE difference, Sb amorphorization may not be the sole/major reason to cycling stability improvement. 2) The more parasitic reactions, SEI formation and large impedance increase of SIBs did not lead to capacity fade. The difference on ion transfer kinetic in SIBs and LIBs did not contribute much to the different cycling stability. 3) The SEI layer has a main function of stabling the electrode-electrolyte interphase, while it is insulating and slows down the ion transfer when it is too thick.[28, 29] However, for the Sb@C MSs in SIBs, thick SEI on the surface did not deter Na-ion transfer and hence did not lead to capacity fade. It is believed the thick SEI, is critical as mechanically robust protecting layer to improve the long-term cycling stability, by mitigating the challenge of volume expandable alloy.[30] The SEM images of cycled electrodes in SIBs (Figures S4-S6) show better preserved spherical morphology than in LIBs.

Conclusion

In summary, we have prepared the pomegranate Sb@C yolk-shell microsphere to improve the long-term cycling stability and packing density. As the SIB anode, it demonstrated an incredible 99.8% capacity retention after 200 cycles and 77% for LIBs. The packing density increased 30% than nano-sized Sb@C yolk-shell structure. Using it as a material platform, we elucidated the SEI effect on the cycling stability difference in LIBs and SIBs. The thick SEI developed on the electrode surface in SIBs did not deter the Na-ion transfer and was very beneficial to the mechanical stability and hence is considered a main reason for the better cyclability. Although it is not practical forming thick SEI in practical full-cell batteries, this study revealed the importance of designing stable SEI for high-density alloy based anode for LIBs and SIBs. The dissimilar SEI properties between Li and Na chemistries also inspire a quest for customized material and electrolyte design for their own respective electrochemical systems.

Supporting Information

Correspondence Author

*E-mail: yuehe.lin@wsu.edu; xiaolin.Li@pnnl.gov

Author Contributions

J.S., Y.L. and X.L. initiated the project. J.S. synthesized the materials. D.X., H.J. and G.Z. conducted

TEM and SEM analyses. J.S. and S.F. performed electrochemical testing. J.S., Y.L. and X.L.

prepared the manuscript with input from all the other co-authors.

REFERENCE

1.   G. H. Newman and L. P. Klemann, *J. Electrochem. Soc.*, 1980, **127**, 2097-2099.
2.   M. Winter, J. O. Besenhard, M. E. Spahr and P. Novak, *Adv Mater*, 1998, **10**, 725-763.
3.   S. Chu and A. Majumdar, *Nature*, 2012, **488**, 294-303.
4.   J. Liu, J. G. Zhang, Z. G. Yang, J. P. Lemmon, C. Imhoff, G. L. Graff, L. Y. Li, J. Z. Hu, C. M. Wang, J. Xiao, G. Xia, V. V. Viswanathan, S. Baskaran, V. Sprenkle, X. L. Li, Y. Y. Shao and B. Schwenzer, *Adv. Funct. Mater.*, 2013, **23**, 929-946.
5.   V. Palomares, P. Serras, I. Villaluenga, K. B. Hueso, J. Carretero-Gonzalez and T. Rojo, *Energ. Environ. Sci.*, 2012, **5**, 5884-5901.
6.   K. Westman, R. Dugas, P. Jankowski, W. G. Wieczorek, G. Gachot, M. Morcrette, E. Irisarri, A. Ponrouch, M. R. Palacin and J.-M. Tarascon, *ACS Applied Energy Materials*, 2018, **1**, 2671-2680.
7.   Z. M. Liu, T. C. Lu, T. Song, X. Y. Yu, X. W. Lou and U. Paik, *Energ. Environ. Sci.*, 2017, **10**, 1576-1580.
8.   J.-I. Lee, J. Song, Y. Cha, S. Fu, C. Zhu, X. Li, Y. Lin and M.-K. Song, *Nano Research*, 2017, **10**, 4398-4414.
9.   H. L. Zhu, Z. Jia, Y. C. Chen, N. Weadock, J. Y. Wan, O. Vaaland, X. G. Han, T. Li and L. B. Hu, *Nano Lett.*, 2013, **13**, 3093-3100.
10.   X. H. Xiong, C. H. Yang, G. H. Wang, Y. W. Lin, X. Ou, J. H. Wang, B. T. Zhao, M. L. Liu, Z. Lin and K. Huang, *Energ. Environ. Sci.*, 2017, **10**, 1757-1763.
11.   W. J. Li, S. L. Chou, J. Z. Wang, J. H. Kim, H. K. Liu and S. X. Dou, *Adv. Mater.*, 2014, **26**, 4037-4042.
12.   N. Liu, Z. D. Lu, J. Zhao, M. T. McDowell, H. W. Lee, W. T. Zhao and Y. Cui, *Nat. Nanotechnol.*, 2014, **9**, 187-192.

13.   X. W. Li, Z. B. Yang, Y. J. Fu, L. Qiao, D. Li, H. W. Yue and D. Y. He, *ACS Nano*, 2015, **9**, 1858-1867.
14.   Y. Jin, S. Sun, M. Ou, Y. Liu, C. Fan, X. Sun, J. Peng, Y. Li, Y. Qiu and P. Wei, *ACS Applied Energy Materials*, 2018, **1**, 2295-2305.
15.   J. Liu, L. T. Yu, C. Wu, Y. R. Wen, K. B. Yin, F. K. Chiang, R. Z. Hu, J. W. Liu, L. T. Sun, L. Gu, J. Maier, Y. Yu and M. Zhu, *Nano Lett.*, 2017, **17**, 2034-2042.
16.   L. T. Yu, J. Liu, X. J. Xu, L. G. Zhang, R. Z. Hu, J. W. Liu, L. C. Yang and M. Zhu, *ACS Appl. Mater. Inter.*, 2017, **9**, 2516-2525.
17.   C. M. Park, J. H. Kim, H. Kim and H. J. Sohn, *Chem Soc Rev*, 2010, **39**, 3115-3141.
18.   A. Darwiche, C. Marino, M. T. Sougrati, B. Fraisse, L. Stievano and L. Monconduit, *J. Am. Chem. Soc.*, 2013, **135**, 10179-10179.
19.   C. K. Chan, H. L. Peng, G. Liu, K. McIlwrath, X. F. Zhang, R. A. Huggins and Y. Cui, *Nat. Nanotechnol.*, 2008, **3**, 31-35.
20.   M. T. McDowell, S. W. Lee, I. Ryu, H. Wu, W. D. Nix, J. W. Choi and Y. Cui, *Nano Lett.*, 2011, **11**, 4018-4025.
21.   J. H. Song, P. F. Yan, L. L. Luo, X. G. Qi, X. H. Rong, J. M. Zheng, B. W. Xiao, S. Feng, C. M. Wang, Y. S. Hu, Y. H. Lin, V. L. Sprenkle and X. L. Li, *Nano Energy*, 2017, **40**, 504-511.
22.   M. H. Lee, Y. Kang, S. T. Myung and Y. K. Sun, *Electrochim Acta*, 2004, **50**, 939-948.
23.   J. M. Zheng, S. J. Myeong, W. R. Cho, P. F. Yan, J. Xiao, C. M. Wang, J. Cho and J. G. Zhang, *Adv. Energy Mater.*, 2017, **7,** 1601284.
24.   L. Baggetto, P. Ganesh, C. N. Sun, R. A. Meisner, T. A. Zawodzinski and G. M. Veith, *J. Mater. Chem. A*, 2013, **1**, 7985-7994.
25.   S. Komaba, W. Murata, T. Ishikawa, N. Yabuuchi, T. Ozeki, T. Nakayama, A. Ogata, K. Gotoh and K. Fujiwara, *Adv. Funct. Mater.*, 2011, **21**, 3859-3867.
26.   L. W. Ji, M. Gu, Y. Y. Shao, X. L. Li, M. H. Engelhard, B. W. Arey, W. Wang, Z. M. Nie, J. Xiao, C. M. Wang, J. G. Zhang and J. Liu, *Adv. Mater.*, 2014, **26**, 2901-2908.
27.   Y. H. Xu, Y. J. Zhu, Y. H. Liu and C. S. Wang, *Adv. Energy Mater.*, 2013, **3**, 128-133.
28.   J. Song, B. Xiao, Y. Lin, K. Xu and X. Li, *Adv. Energy Mater.*, 2018, **8**, 1703082.
29.   K. Xu, *Chemical Reviews*, 2014, **114**, 11503-11618.
30.   A. Darwiche, L. Bodenes, L. Madec, L. Monconduit and H. Martinez, *Electrochim Acta*, 2016, **207**, 284-292.

Micron yolk-shell Sb@C
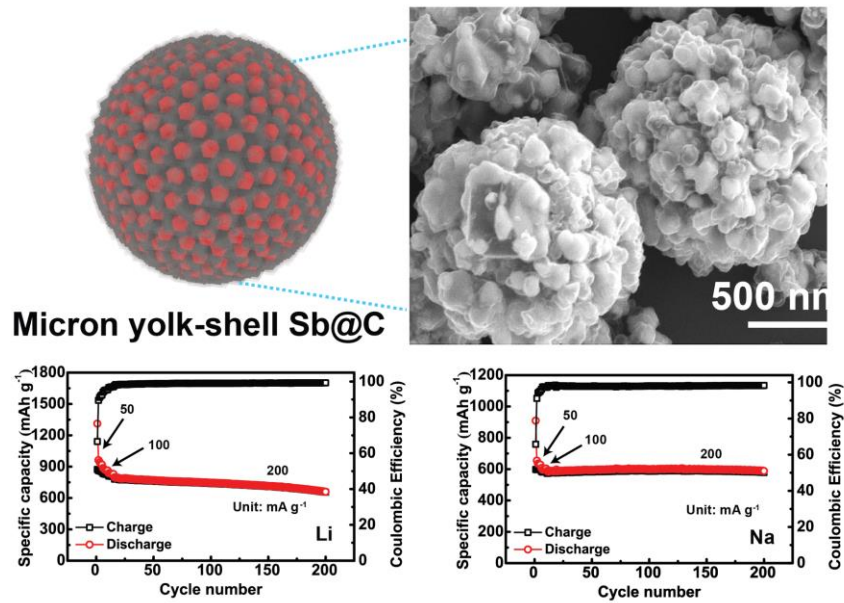
High packing density pomegranate Sb@C yolk-shell structure has been developed as high-performance anodes for lithium-ion and sodium-ion batteries